

PAPER



Cite this: *Dalton Trans.*, 2016, **45**, 8566

Received 3rd March 2016,
Accepted 6th April 2016

DOI: 10.1039/c6dt00859c

www.rsc.org/dalton

$\{\text{Ni}_8\text{Ln}_6\}$ (Ln = Gd, Dy) rod-like nano-sized heteronuclear coordination clusters with a double carbonate bridge skeleton and remarkable MCE behaviour†

Eliana Guarda,^a Katharina Bader,^b Joris van Slageren^b and Pablo Alborés*^a

The newly obtained complexes $[\text{Ni}_8\text{Ln}_6^{\text{III}}(\text{Piv})_{16}(\text{teaH})_6(\text{OCH}_3)_2(\text{CO}_3)_2(\text{H}_2\text{O})_2]$ Ln = Gd, Dy, show a remarkable μ_5 -carbonate bridged octanuclear planar $\{\text{Ni}_4\text{Ln}_4\}$ core further capped with embedded $\{\text{Ni}_3\text{Ln}\}$ cubane motifs to afford a rod shaped nano-sized molecule of about 1.2×2.8 nm. Unusual MCE behaviour has been found due to multiple low lying excited states arising from competing ferromagnetic and anti-ferromagnetic Ni–Ni and Ni–Ln exchange interactions.

Introduction

Recently, the development of carbonate chemistry in the context of 3d/4f polynuclear compound synthesis has been remarkable. It was shown that the number of structurally characterized non-polymeric 3d/4f compounds bearing at least one carbonate ligand is still very small.¹ The huge cages, $\text{Ni}_{54}\text{Gd}_{54}$ and $\text{Ni}_{30}\text{La}_{20}$, appear as the highest nuclearity structurally characterized reported examples within this family.² There is a gap then from these giant clusters followed by a $\text{Cu}_{15}\text{Gd}_7$ example³ and then by Co_8Ln_6 and $\text{Ni}_{12}\text{Ln}_2$ systems,⁴ showing that these huge clusters are still very scarce. High nuclearity complexes combining 3d metals and 4f lanthanides, are continuously being explored as potential nanomagnets, which offer fascinating properties such as SMM behaviour⁵ or MCE features.⁶ Carbonate inclusion through air CO_2 fixation remains a versatile route in the assembly of this type of system. In this work, we have explored the reaction of a pivalate nickel precursor $\text{Ni}_2(\mu\text{-H}_2\text{O})(\text{Piv})_4(\text{HPiv})_4$ with lanthanide nitrate and the versatile triethanolamine polydentate ligand under an open atmosphere. We have found that smooth reaction conditions afford high nuclearity complexes bearing Ni_8Ln_6 metallic cores and carbonate bridges. Herein, we report

their structural characterization as well as a preliminary magnetic study.

Results and discussion

Synthesis and structural characterization

The room temperature smooth reaction of $\text{Ni}_2(\mu\text{-H}_2\text{O})(\text{Piv})_4(\text{HPiv})_4$ and $\text{Ln}(\text{NO}_3)_3 \cdot x\text{H}_2\text{O}$ (or $\text{Y}(\text{NO}_3)_3 \cdot x\text{H}_2\text{O}$) with teaH_3 under aerobic conditions in a methanol/acetonitrile mixture and the presence of triethylamine as a base, afforded extremely pale green, almost colourless, plate-like crystals of the compounds: $[\text{Ni}_8\text{Ln}_6^{\text{III}}(\text{Piv})_{16}(\text{teaH})_6(\text{OCH}_3)_2(\text{CO}_3)_2(\text{H}_2\text{O})_2]$ Ln = Gd(1), Dy(2), Piv = trimethylacetate; teaH_3 = triethanolamine, as well as the isostructural $[\text{Ni}_8\text{Y}_6^{\text{III}}(\text{Piv})_{16}(\text{teaH})_6(\text{OCH}_3)_2(\text{CO}_3)_2(\text{H}_2\text{O})_2]$ (3). The stoichiometric teaH_3 :Ni relationship appears critical and a value higher than 2 affords exclusively the previously characterized mononuclear $[\text{Ni}(\text{teaH}_3)_2](\text{Piv})_2$ as huge blue single crystals.⁷ Efforts to increase the low product yield, as for example employing CO_2 gas bubbling through the reaction mixture, proved unsuccessful. Further evaporation of mother liquors after crystal collection only afforded the above mentioned blue crystals after several weeks.

These new complexes, with a total of fourteen metal centers, are placed within the group of highest nuclearity examples among the Ni(II)–Ln(III) carbonate bridged family^{2,4b,8} levelling the previously reported $\text{Ni}_{12}\text{Ln}_2$ compounds.^{4b} Surprisingly, they become the first example of a Ni_8Ln_6 stoichiometry among all the previously reported Ni/Ln complexes.

Compounds 1–3 are isostructural with minor geometrical deviations; hence we report here a single structural description. The structure (Fig. 1) is that of a heterometallic 3d/4f complex consisting of eight Ni(II) and six Ln(III) ions (or Y(III)),

^aDepartamento de Química Inorgánica, Analítica y Química Física/INQUIMAE (CONICET), Facultad de Ciencias Exactas y Naturales Universidad de Buenos Aires, Pabellón 2, Ciudad Universitaria, C1428EHA Buenos Aires, Argentina.
E-mail: albores@qi.fcen.uba.ar; Tel: +54 (0)1145763380

^bInstitut für Physikalische Chemie, Universität Stuttgart, Pfaffenwaldring 55, D-70569 Stuttgart, Germany

† Electronic supplementary information (ESI) available. CCDC 1453963–1453965. For ESI and crystallographic data in CIF or other electronic format see DOI: 10.1039/c6dt00859c

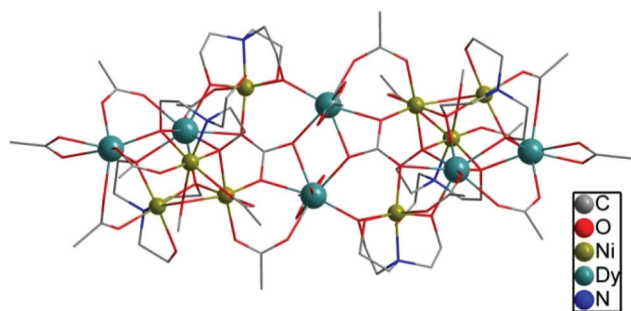


Fig. 1 Molecular representation of Ni_8Dy_6 . *tert*-Butyl groups and H atoms have been omitted for the sake of clarity.

with the asymmetric unit of the monoclinic $P21/n$ cell consisting of half of the molecule which lies on a crystallographic inversion centre, thus making both $\{\text{Ni}_4^{\text{II}}\text{Ln}_3^{\text{III}}\}$ cores symmetry-equivalent. Two methanol and one acetonitrile solvent molecules complete the whole asymmetric unit content. The whole molecule has a rod-like shape with dimensions of *ca.* 1.2 nm \times 2.8 nm entering the nano-scale world (see the ESI†). The $\{\text{Ni}_8^{\text{II}}\text{Ln}_6^{\text{III}}\}$ core mirrors this rod-like arrangement with an unprecedented central double μ_5 -carbonate bridged octanuclear $\{\text{Ni}_4\text{Ln}_4\}$ moiety (see the ESI†). There are no examples of previously reported 3d/4f compounds showing this particular double μ_5 -carbonate bridged octanuclear moiety. In fact the only examples that can be found are those with $\{\text{Na}_4\text{Ln}_4\}$ units.⁹

Two embedded $\{\text{Ni}_2\text{Ln}\}$ units at both edges, configuring capped opened cubane motifs, complete the metallic core of the molecule. When looking more closely at the central $\{\text{Ni}_4^{\text{II}}\text{Ln}_4^{\text{III}}\}$ subunit, four μ_2 -pivalates and eight μ_2 -alkoxides from the triethanolamine ligands can be observed, in addition to the main double carbonate bridge. The terminal capped opened cubane motif (equivalent by symmetry at both sides of the central octanuclear core) is held together through three μ_2 -pivalates, four μ_3 -alkoxides from the triethanolamine ligands and one μ_3 -methoxide. It is then further connected to the $\{\text{Ni}_4^{\text{II}}\text{Ln}_4^{\text{III}}\}$ central unit through the carbonate bridge. The opened cubane structure is built up with a $\{\text{Ni}_3\text{Ln}\}$ unit (see the ESI†) and an additional Ln(III) ion in the capping position. Four η_2 -pivalate and two aqua ligands complete the whole molecular structure. In order to analyse the local coordination environment of the metal centers it is enough to look at half a molecule due to the inversion center. All Ni(II) centers are six coordinated, with $[\text{NO}_5]$ donor atom sets in the case of Ni(1), Ni(2), and Ni(4) and $[\text{O}_6]$ in the case of Ni(3). Ni(4), embedded in the central octanuclear core, as well as Ni(2) and Ni(3) which are part of the capped open cubane motif, show a set of five short Ni–L bond distances in the range of 2.024(9)–2.10(1) Å and a unique long Ni–L bond distance ranging from 2.128(8) to 2.17(1) Å. On the other hand, Ni(1), placed at a corner of the opened cubane moiety, shows a set of four in-plane short Ni–L bond distances ranging from 2.021(9) to 2.107(9) Å and two long Ni–L bond distances ranging from 2.123(7) to 2.15(1) Å, Ni–O, and 2.12(1)–2.15(1)

Å, Ni–N. Summarizing, all Ni(II) sites display axial elongated distorted octahedral environments, with Ni(1) as the most axial elongated site.

Concerning Ln(III) (or Y(III)) sites, as expected, all of them are bound to O donor atoms, with a coordination number of seven for Ln(1) and eight in the case of Ln(2) and Ln(3). Employing the SHAPE¹⁰ routine the following closest geometries are found: a capped trigonal prism (CShM = 2.029 (1, Gd); 2.007 (2, Dy); 2.023 (3, Y)), Ln(1) (or Y(1)); a bicapped trigonal prism (CShM = 1.809 (1, Gd); 1.826 (2, Dy); 1.871 (3, Y)), Ln(2) (or Y(2)) and a triangular dodecahedron (CShM = 3.154 (1, Gd); 2.865 (2, Dy); 2.888 (3, Y)), Ln(3) (or Y(3)). These correspond to local symmetries: C_{2v} for Ln(1) (or Y(1)) and Ln(2) (or Y(2)) and D_{2d} for Ln(3) (or Y(3)). As can be seen from these CShM values, all Ln(III) (or Y(III)) environments are somehow distorted from the idealized geometries. The Ln–O (or Y–O) bond distances at each different site span an overall quite narrow range: 2.290(5)–2.472(9) Å (mean value of 2.35(7) Å), (1, Gd); 2.19(1)–2.42(2) Å (mean value of 2.30(1) Å), (2, Dy); 2.22(1)–2.46(2) Å (mean value of 2.31(1) Å), (3, Y) for Ln(1) (or Y(1)) site; 2.275(6)–2.589(6) Å (mean value of 2.426(6) Å), (1, Gd); 2.257(9)–2.59(1) Å (mean value of 2.40(1) Å), (2, Dy); 2.261(9)–2.59(1) Å (mean value of 2.39(1) Å), (3, Y) for Ln(2) (or Y(2)) site and 2.231(6)–2.484(5) Å (mean value of 2.395(6) Å), (1, Gd); 2.21(1)–2.452(9) Å (mean value of 2.372(9) Å), (2, Dy); 2.21(1)–2.460(9) Å (mean value of 2.36(1) Å), (3, Y) for Ln(3) (or Y(3)) site. When looking at the mean Ln–O (including Y–O) values at all sites they span the range of 2.30(1)–2.426(6) Å.

Remarkably, along the main molecular rod skeleton, all Ln(III) (or Y(III)) sites appear connected through the double carbonate bridging system and two further terminal double μ_2 -alkoxide μ_2 -carboxylate bridges. Hence the whole molecular core can alternatively be described as a rod-like double carbonate bridged hexanuclear Ln(III) moiety peripherally decorated with eight Ni(II) ions.

As frequently found in carboxylate based clusters, intramolecular H-bonding interactions are observed, involving the coordinated aqua ligands and teaH^{2-} ligands (see the ESI†).

Regarding the molecular crystal packing (see the ESI†), these nano-rods are piled along the monoclinic *b*-axis creating a columnar arrangement, held together by H-bond interactions between the neighbouring O atoms of the κ^2 -carboxylate ligand and a free-pendant teaH^{2-} arm. This affords the shortest intermolecular metal–metal distances of Ni(1)⋯Ln(1)/Y(1), 7.912(1) Å (1, Gd); 7.957(2) Å (2, Dy); 7.989(3) Å (3, Y), with the shortest Ln(1)/Y(1)⋯Ln(1)/Y(1) distances of 8.8360(9) Å (1, Gd); 8.884(1) Å (2, Dy); 8.923(3) Å (3, Y) and the shortest Ni(1)⋯Ni(1) distances of 8.616(2) Å (1, Gd); 8.618(2) Å (2, Dy); 8.646(3) Å (3, Y). The main axis of the molecular rod makes an angle of *ca.* 36° with respect to the *b*-axis direction. Moreover, the main axes of the columns are not completely aligned among them, but alternatively tilted also with an angle of about 36°. The bulky *tert*-butyl groups keep these columns of rods well apart from each other at *ca.* 15 Å, estimated from the closest carbonate C atoms of neighbouring columns. The solvent molecules are not involved in short contact interactions, they simply fill voids.

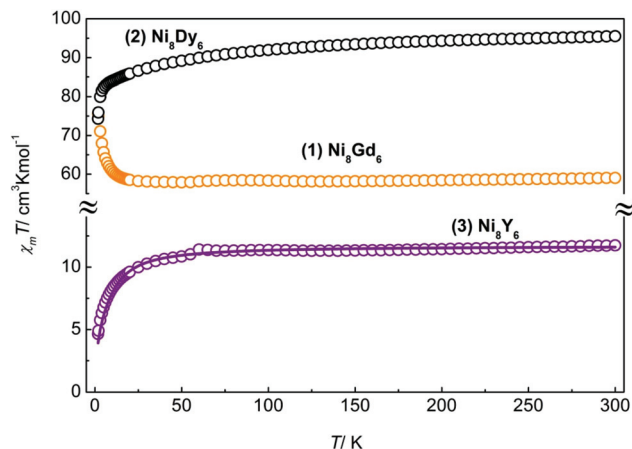


Fig. 2 $\chi_m T$ vs. T data plot at 1 kOe in 2–300 K range of complexes 1–3. Open circles: experimental; full line: fitted (see the text).

Magnetic properties

To investigate the magnetic properties, direct current (DC) magnetic susceptibility measurements were performed on ground single crystal crops of compounds 1–3 in the temperature range of 2–300 K and in an applied field of 1 kOe (Fig. 2). In addition, magnetisation measurements were carried out at different temperatures (1.8–10 K) in the range of 0–70 kOe (Fig. 3).

From the magnetic perspective, the Ni_8Y_6 complex (3) is an invaluable reference because of the closed-shell nature of $\text{Y}(\text{III})$. Magnetically, 3 is a $\text{Ni}(\text{II})$ cluster, which is easier to analyze than the $\text{Ln}(\text{III})$ analogues.

The observed room temperature $\chi_m T$ value of 3 is $11.8 \text{ cm}^3 \text{ K mol}^{-1}$, which is in agreement with the theoretical value for eight non-interacting $\text{Ni}(\text{II})$ ions ($S = 1$) with $g = 2.43$. This g value is at the upper end of the normal range for $\text{Ni}(\text{II})$.¹¹ Upon cooling, the $\chi_m T$ value falls gradually, down to $\sim 50 \text{ K}$, before plummeting to reach a value of $4.6 \text{ cm}^3 \text{ mol}^{-1} \text{ K}$ at 1.8 K. This behaviour suggests dominant anti-ferromagnetic

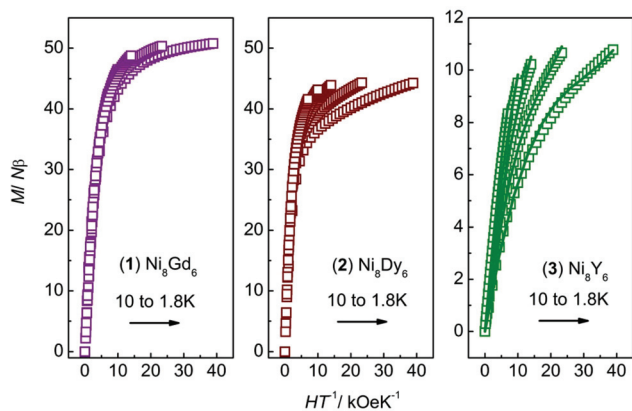


Fig. 3 M vs. HT data plot in the range of 0–70 kOe at temperatures between 1.8 and 10 K of complexes 1–3. Open squares: experimental; full line: fitted (see the text).

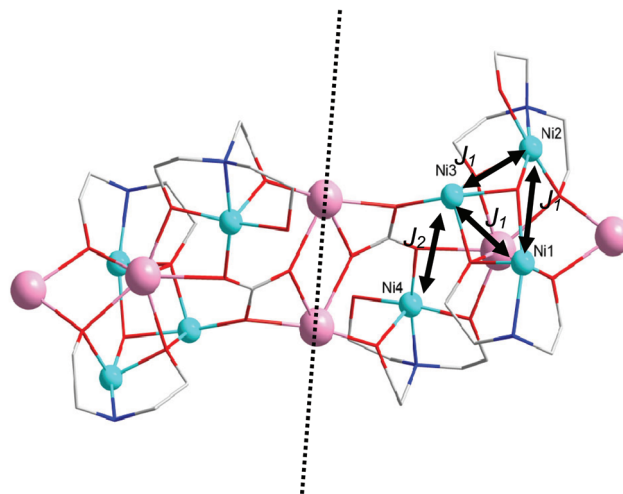


Fig. 4 Spin topology and simplified exchange interaction pattern employed in the magnetic data analysis of complex Ni_8Y_6 . Pink: closed shell $\text{Y}(\text{III})$ sites.

interactions within $\text{Ni}(\text{II})$ ions, in possible conjunction with sizable zero-field splitting. The reduced magnetisation data show no saturation behaviour suggesting the absence of a well isolated ground spin state. In fact, the increase of magnetisation when temperature is increased evidences low lying spin multiplets of a higher magnitude than the ground state.

To further understand this behaviour, a closer inspection of the spin topology must be performed (Fig. 4). The central diamagnetic double carbonate bridged $\{\text{Y}(\text{III})_2\}$ unit undoubtedly leads to magnetic decoupling of the $\{\text{Ni}_8\}$ cluster into two symmetry equivalent $\{\text{Ni}_4\}$ ones, simplifying the interpretation of the magnetic behaviour. These $\{\text{Ni}_4\}$ units represent an atypical topology: a multiple alkoxo bridged triangular $\{\text{Ni}_3\}$ core with a μ_2 - $(\eta^1\text{-syn-}\eta^1\text{-anti})$ carbonate bridged single $\text{Ni}(\text{II})$ site.

In principle four different exchange pathways can be identified: the three within the $\{\text{Ni}_3\}$ triangle and a fourth carbonate mediated between $\text{Ni}(1)$ (triangle member) and $\text{Ni}(4)$. However, it is not possible to extract all these parameters from experimental data avoiding over-parametrization. We found that the minimum set of parameters able to properly reproduce magnetic susceptibility data involves a unique exchange interaction within all three $\text{Ni}(\text{II})$ ions within the triangle and a second one for the μ -carbonate pathway:

$$\hat{H} = -2J_1(\hat{S}_1\hat{S}_2 + \hat{S}_1\hat{S}_3 + \hat{S}_2\hat{S}_3) - 2J_2\hat{S}_1\hat{S}_4 \quad (1)$$

We employed the PHI package¹² to obtain the best fitting parameters from experimental data. Thus, we attempted a simultaneous fitting of susceptibility and magnetisation experimental data. Through this approach we succeeded in obtaining a consistent set of final parameters: $g = 2.42$, $J_1 = -2.3 \text{ cm}^{-1}$ and $J_2 = 3.9 \text{ cm}^{-1}$. Most probably, the low temperature data is affected by zero-field splitting of the individual $\text{Ni}(\text{II})$ ions. However, severe over-parametrization problems prevent extracting this information confidently.

The obtained values for the exchange coupling constants are in agreement with other related observed systems. It has been shown that the sign of the interaction is determined by the Ni–O–Ni angle, with angles close to 98° as the turning point.¹³ The presence of multiple bridging pathways makes the analysis more complex, but it could be possible that anti-ferromagnetic and ferromagnetic interactions overlap within the $\{\text{Ni}_3\}$ triangle due to the asymmetry of the involved Ni–O–Ni angles (Ni–O–Ni angles (degrees) in Ni_8Y_6 are: Ni(1)/Ni(3), 88.7(4), 94.8(4); Ni(2)/Ni(3), 93.8(4), 98.0(4); Ni(1)/Ni(2), 128.8(5)). In the case of the carbonate bridged pathway there are no examples reported for (η^1 -*syn*- η^1 -*anti*)carbonate bridged Ni(II) ions for comparison. However, for other possible carbonate bridging modes, some reports can be found for Ni(II) compounds, showing exchange interactions of a few wavenumbers in agreement with the *a priori* unexpected high value found in complex 3.¹⁴ The lack of other examples prevents a deeper discussion about this exchange pathway thus quantum calculations will probably be most helpful.

The ground state arising from the fitted exchange interactions corresponds to an $S = 1$, with degenerate $S = 0$, $S = 2$ states at only 3 cm^{-1} , and with all the multiplet ladders condensed in a narrow range of 45 cm^{-1} (see the ESI†).

Magnetic data analysis of the $\{\text{Ni}_8\text{Ln}_6\}$ complexes 1 and 2 is much more complicated due to the additional exchange pathways between Ni(II) and Ln(III) sites that break the simplified two identical isolated $\{\text{Ni}_4\}$ units model.

The observed room temperature $\chi_{\text{m}}T$ values are $59.1 \text{ cm}^3 \text{ K mol}^{-1}$ (1) and $95.5 \text{ cm}^3 \text{ K mol}^{-1}$ (2), in reasonable agreement with the expected $\chi_{\text{m}}T$ value for eight non-interacting Ni(II) ions ($S = 1$) with a $g = 2.42$ and six Ln(III): $58.9 \text{ cm}^3 \text{ K mol}^{-1}$ (Gd, 1, $S = 7/2$, $g = 2$) and $96.9 \text{ cm}^3 \text{ K mol}^{-1}$ ($\chi_{\text{m}}T = 14.2 \text{ cm}^3 \text{ mol}^{-1} \text{ K}$ for a Dy(III) ion with spherical symmetry). In the case of complex 2, this agreement shows that at rt, Dy(III) crystal field split m_j levels are almost equally populated. Following this complex, upon cooling, the $\chi_{\text{m}}T$ value falls more quickly than for complex 3, due to Dy(III) sites m_j level depopulation, up to *ca.* 80 K where it abruptly further decreases to reach a final $\chi_{\text{m}}T$ value of $74.3 \text{ cm}^3 \text{ K mol}^{-1}$ at 1.8 K. This behaviour is ascribed to dominant Ni(II) exchange interactions (already analysed in complex 3) over the weaker Ni(II)–Dy(III) ones. The reduced magnetisation data profile looks similar to that observed for complex 3 with no saturation onset, suggesting again dominating Ni(II) exchange interactions at low temperature, mostly unperturbed by Dy(III) sites. The highest achieved M value of about $44N\beta$ is well below the expected value for the six uncoupled Dy(III) ions in spherical symmetry ($60N\beta$), reflecting the high crystal field anisotropy of these Ln(III) ions, as the exchanged Ni(II) ions contribution is yet to be added to this value ($11N\beta$ if Ni_8Y_6 magnetisation data is replicated).

The $\chi_{\text{m}}T$ vs. T profile of complex 1 is clearly different from that observed in compounds 2 and 3. $\chi_{\text{m}}T$ smoothly decreases from 300 K to 30 K (62.0 to $58.4 \text{ cm}^3 \text{ K mol}^{-1}$), where it suddenly increases to reach a final value of $75.6 \text{ cm}^3 \text{ K mol}^{-1}$ at 1.8 K. This points to the onset of non-negligible ferromagnetic Gd(III)–Ni(II) and/or Gd(III)–Gd(III) exchange interactions, giving

rise to a high spin ground state multiplet. The reduced magnetisation data profile is also different from the corresponding profile of complexes 2 and 3, as incipient saturation is observed at the lowest temperature data with a value of $51N\beta$. This value could be compatible with a total S for the ground state close to 25. However, as observed in the Ni_8Y_6 and Ni_8Dy_6 compounds, the magnetisation increases with increasing temperature at a fixed field, suggesting the absence of an isolated ground state. In this sense, the maximum achieved magnetisation value can be arising from a low lying excited state with a higher S value than the zero field ground state. This observation agrees with the moderate magnitude of the exchange interactions between Ni(II) ions and the usually observed between 3d metals and Ln(III) ions, of a few wavenumbers.¹⁵

The huge size of the spin system of complex 1 (eight $S = 1$ and six $S = 7/2$, $\sim 10^8$ matrix dimension) precludes any attempt of magnetic data simulation with a complete exchange HDVV spin Hamiltonian by standard methods. It proved also impossible to account for the magnetisation data supposing an isolated ground state with a total spin, S , supporting the hypothesis about the presence of several low lying energy spin multiplets above the ground state one.

In the case of the Ni_8Dy_6 complex no slow relaxation of magnetisation could be detected through AC susceptibility measurements even in the presence of a low DC external magnetic field, in contrast to what has been observed for many Dy(III) complexes.

The possible high spin ground state of complex 1, together with several low lying excited state multiplets, prompted us to evaluate its MCE (magnetocaloric effect) properties. We employed magnetisation data to estimate the MCE, making use of the Maxwell equation:

$$\Delta S_{\text{m}}(T, \Delta H) = \int_{H_1}^{H_2} \left(\frac{\partial M}{\partial T} \right)_H dH \quad (2)$$

We explored the magnetic entropy change at different fields in the range of 2–10 K (Fig. 5). The observed maximum in the temperature dependence drastically shifts to higher temperatures on increasing magnetic field change. In fact at some

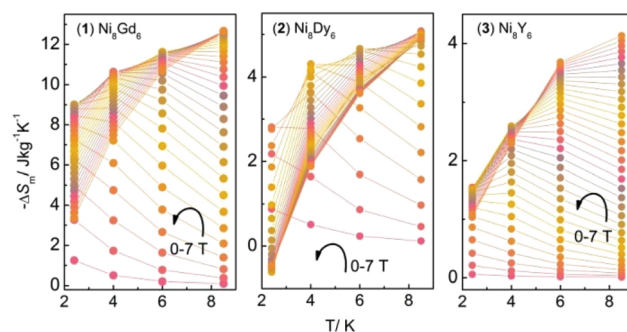


Fig. 5 Temperature-dependency of the magnetic entropy change ΔS_{m} for the indicated applied-field changes, as obtained from magnetization measurements of complexes 1–3. Arrows indicate the profile evolution with increasing field change.

critical field range (between 2 and 4 T, see the ESI†), the magnetic entropy change starts increasing with higher temperatures. This suggests the existence of several low lying excited states that provoke subsequently level crossings. There are no reports, to the best of our knowledge, of this striking behaviour where such switching MCE with magnetic field has been observed in molecular systems.

The maximum ΔS_m reached is $12.6 \text{ J kg}^{-1} \text{ K}^{-1}$ at 8.5 K for a 0–7 T field change. This value is clearly lower than that expected for eight isolated Ni(II) ions and six isolated Gd(III) ones ($42.8 \text{ J kg}^{-1} \text{ K}^{-1}$). This is expected as the whole exchange split multiplet ladder spans more than 30 cm^{-1} in energy (at least considering the exchange coupling constants obtained for the Ni_8Y_6 complex). However, it is higher than the maximum values expected for isolated ground states between $S = 22\text{--}25$, which should be in the range of $7.65\text{--}7.9 \text{ J kg}^{-1} \text{ K}^{-1}$. This suggests an enhanced MCE of the high spin ground state due to low lying excited multiplets, in agreement with magnetisation data discussion. The entropy change value observed becomes valuable when considering the high molecular mass of complex **1** and in comparison with the highest reported entropy changes in 3d/4f molecular nanomagnets.⁶

It is interesting to compare this MCE effect with those observed in the Ni_8Y_6 and Ni_8Dy_6 compounds. As expected, complex **1** shows much lower entropy change values, but still preserves the temperature-field dependence profile. It seems that the Ni(II)–Ni(II) exchange pathways play a key role in this distinctive feature. As for complex **1**, the maximum ΔS_m reached $4.1 \text{ J kg}^{-1} \text{ K}^{-1}$ at 8.5 K for a 0–7 T field change, and is well below the expected value for eight uncoupled Ni(II) ions ($29.5 \text{ J kg}^{-1} \text{ K}^{-1}$). However it is almost coincident with the expected value for two uncorrelated $S = 1$ total ground states (arising from two Ni_4 units), $4.9 \text{ J kg}^{-1} \text{ K}^{-1}$.

The replacement of Y(III) with Dy(III) adds no entropy change contribution but strongly diminishes it at lower temperatures. This could be probably explained in terms of the highly anisotropic nature of the Dy(III) ion. At higher temperatures the profile is almost coincident with that observed for complex **1**, proving the almost negligible exchange interaction between Ni(II) and Dy(III) sites. The temperature dependence profile is preserved with a notable maximum shifting (more than 5 K) and the striking feature is that at the highest field and lowest temperature, the sign of the entropy change is reversed. We have found no reports of this behaviour in nanomagnet systems.

This peculiar behaviour could be ascribed to the combination of low magnetic entropy contribution at zero field of ground Kramers doublets of the Dy(III) ions together with the field induced low lying excited multiplet (arising from Ni(II)–Ni(II) exchange interaction) magnetic entropy contribution.

Conclusions

In summary, we have shown that CO_2 air fixation is a versatile tool in the assembly of high nuclearity Ni(II)–Ln(III) complexes

due to its multiple bridging mode capability. In the reported examples, the weak to moderate exchange interactions between Ni(II) sites configure a low lying excited multiplet energy ladder. The inclusion of Ln(III) ion activates Ni(II)–Ln(III) exchange pathways, ferromagnetic in the case of Gd(III) but anti-ferromagnetic in the case of Dy(III). The final competing exchange interactions promote an atypical MCE behaviour where temperature dependence of entropy change switches at a critical external field. Further studies must be performed in order to gain a deeper insight into this magnetic behaviour.

Experimental section

Materials and physical measurements

$[\text{Ni}_2(\mu\text{-OH})_2(\mu\text{-Piv})_2(\text{Piv})_2(\text{HPiv})_4]$, Piv = trimethylacetate, was prepared following a previously reported procedure.¹⁶ $\text{Ln}(\text{NO}_3)_3 \cdot x\text{H}_2\text{O}$ and $\text{Y}(\text{NO}_3)_3 \cdot x\text{H}_2\text{O}$ were prepared from the respective oxides and nitric acid through standard procedures. All other chemicals were reagent grade and used as received without further purification. Elemental analyses for C, H and N were performed with a Carlo Erba 1108 analyzer.

Synthesis of complexes

Synthesis of $[\text{Ni}_8^{\text{II}}\text{Ln}^{\text{III}}(\text{Piv})_{16}(\text{teaH})_6(\text{OCH}_3)_2(\text{CO}_3)_2(\text{H}_2\text{O})_2]$, Ln = Gd(1**), Dy(**2**).** $\text{Ni}_2(\text{OH})_2(\text{Piv})_4(\text{HPiv})_4$ (100 mg, 0.1 mmol) were dissolved in 5 mL of MeCN. To this pale green solution were added triethanolamine (41 mg, 0.28 mmol) and triethylamine (128 mg, 1.3 mmol) previously dissolved in 5 mL of MeCN. Immediately after mixing, a pale solid is formed and re-dissolved by addition of a few drops of methanol under continuous stirring. To this resulting new solution $\text{Ln}(\text{NO}_3)_3 \cdot x\text{H}_2\text{O}$ (76 mg, ~ 0.15 mmol) dissolved in 5 mL of methanol were further added under stirring. The final mixture was then stirred for an hour, filtered and allowed to stand for slow evaporation at room temperature. Within 1–2 weeks a crop of very pale green plates of the final product had crystallized with an average yield of 10%, *ca.* 10 mg, based on Ni.

Anal. Calculated (found) for $\text{C}_{120}\text{H}_{232}\text{Ln}_6\text{N}_6\text{Ni}_8\text{O}_{60}$ C, 34.9 (34.3); H, 5.7(5.6); N, 2.0 (2.2) (**1**); C, 34.6 (34.3); H, 5.6(5.3); N, 2.0 (2.1) (**2**).

Synthesis of $[\text{Ni}_8^{\text{II}}\text{Y}^{\text{III}}(\text{Piv})_{16}(\text{teaH})_6(\text{OCH}_3)_2(\text{CO}_3)_2(\text{H}_2\text{O})_2]$ (3**).** It was prepared in the same manner as compounds **1** and **2** but using $\text{Y}(\text{NO}_3)_3 \cdot x\text{H}_2\text{O}$ instead of Ln(III) nitrate. Average yield: 8%, *ca.* 8 mg, based on Ni.

Anal. Calculated (found) for $\text{C}_{120}\text{H}_{232}\text{Y}_6\text{N}_6\text{Ni}_8\text{O}_{60}$ C, 38.7 (38.1); H, 6.3 (6.2); N, 2.3 (2.4).

Magnetic measurements

Magnetic measurements were performed with a Quantum Design MPMS XL-7 SQUID magnetometer over finely ground crystal samples. All experimental magnetic data were corrected for the diamagnetism of the sample holders and of the constituent atoms (Pascal's tables). DC measurements were conducted from 1.8 to 300 K at 1 kOe and between 1.8 and 10 K in the range of 1–70 kOe.

Table 1 Crystallographic data for 1–3

	1	2	3
Empirical formula	C ₁₂₀ H ₂₃₂ Gd ₆ N ₆ Ni ₈ O ₆₀	C ₁₂₈ H ₂₅₄ Dy ₆ N ₈ Ni ₈ O ₆₄	C ₁₂₈ H ₂₅₄ N ₈ Ni ₈ O ₆₄ Y ₆
Formula weight	4132.14	4374.06	3932.39
<i>T</i> (K)	170(2)	170(2)	170(2)
Crystal system	Monoclinic	Monoclinic	Monoclinic
Space group	<i>P</i> 2 ₁ / <i>n</i>	<i>P</i> 2 ₁ / <i>n</i>	<i>P</i> 2 ₁ / <i>n</i>
<i>a</i> (Å)	16.8021(8)	16.7221(8)	16.7260(18)
<i>b</i> (Å)	19.3423(5)	19.3206(7)	19.3040(18)
<i>c</i> (Å)	28.0775(9)	27.9064(9)	27.980(2)
β (°)	105.489(5)	105.797(4)	105.885(9)
<i>V</i> (Å ³)	8793.5(6)	8675.5(6)	8689(1)
<i>Z</i>	2	2	2
<i>D</i> _{calc} (mg m ⁻³)	1.561	1.674	1.503
Absorption coefficient (mm ⁻¹)	3.138	3.477	2.905
<i>F</i> (000)	4164	4420	4096
λ (Å)	0.71073	0.71073	0.71073
θ Range data collection (°)	3.64–26.0	3.53–27.0	3.53–26.0
Index ranges	–20 ≤ <i>h</i> ≤ 20 –23 ≤ <i>k</i> ≤ 12 –34 ≤ <i>l</i> ≤ 19	–21 ≤ <i>h</i> ≤ 21 –20 ≤ <i>k</i> ≤ 24 –35 ≤ <i>l</i> ≤ 35	–20 ≤ <i>h</i> ≤ 20 –23 ≤ <i>k</i> ≤ 15 –34 ≤ <i>l</i> ≤ 34
Reflections collected/unique	29 962/17 129	55 995/18 682	38 634/17 026
<i>R</i> _{int}	0.0530	0.1056	0.2401
Observed reflections [<i>I</i> > 2σ(<i>I</i>)]	11 094	10 523	5538
Completeness (%)	99.3	99.7	99.7
Maximum/minimum transmission	1.0000/0.57121	1.000/0.51091	1.0000/0.75852
Data/restraints/parameters	17 129/46/877	18 682/66/926	17 026/105/934
Goodness-of-fit (GOF) on <i>F</i> ²	1.054	1.025	0.998
Final <i>R</i> -index [<i>I</i> > 2σ(<i>I</i>)]/all data	0.0705/0.1158	0.0861/0.1597	0.1220/0.2959
w <i>R</i> index [<i>I</i> > 2σ(<i>I</i>)]/all data	0.14693/0.1670	0.1964/0.2504	0.2405/0.3492
Largest peak and hole (e Å ⁻³)	–1.893 and 2.717	2.277 and –4.624	1.841 and –1.289
Weights, <i>w</i>	1/[σ ² (<i>F</i> _o ²) + (0.0595 <i>P</i>) ² + 29.6334 <i>P</i>] where <i>P</i> = (<i>F</i> _o ² + 2 <i>F</i> _c ²)/3	1/[σ ² (<i>F</i> _o ²) + (0.0921 <i>P</i>) ² + 130.1256 <i>P</i>] where <i>P</i> = (<i>F</i> _o ² + 2 <i>F</i> _c ²)/3	1/[σ ² (<i>F</i> _o ²) + (0.1025 <i>P</i>) ²] where <i>P</i> = (<i>F</i> _o ² + 2 <i>F</i> _c ²)/3

MCE measurements

Magnetic entropy changes were indirectly approximated according to the Maxwell equation (see the text), extracting experimental data from the magnetization at variable field and temperature measurements. The Maxwell equation was resolved by numerical integration of the derivative of magnetization with respect to temperature in practical terms, where the integral is replaced by finite differences.

X-ray structure determination

Crystal structures of compounds 1–3 were determined with an Oxford Xcalibur, Eos, Gemini CCD area-detector diffractometer using graphite-monochromated Mo-K α radiation ($\lambda = 0.71069$ Å) at 170 K. Data was corrected for absorption with CrysAlisPro, Oxford Diffraction Ltd, Version 1.171.33.66, applying an empirical absorption correction using spherical harmonics, implemented in the SCALE3 ABSPACK scaling algorithm.¹⁷ The structure was solved by direct methods with SIR97¹⁸ and refined by full-matrix least-squares on *F*² with SHELXL-2014¹⁹ using the WinGX platform.²⁰ Hydrogen atoms were added geometrically and refined as riding atoms with a uniform value of *U*_{iso}. In all structures, most pivalate methyl groups were found disordered around two positions and were refined with 0.5 : 0.5 fixed occupancy factors. In the case of structure 1, solvent methanol and acetonitrile molecules were found severely disordered. Hence, the SQUEEZE algorithm²¹ was employed to remove their contri-

bution to the density map. The voids found were in perfect agreement with solvent positions in structures 2 and 3.

In the case of structure 2, one pivalate ligand showed disorder over the C and one O of the carboxylate moiety. They were refined over two split positions with 0.5 : 0.5 fixed occupancy factors.

In the case of structure 3, the methoxide methyl and teaH₃ methylenes were also found disordered around two positions and were also refined with 0.5 : 0.5 fixed occupancy factors.

Final crystallographic data and values of *R*₁ and w*R* are listed in Table 1. CCDC 1453963–1453965 contain the supplementary crystallographic data for this paper.

Powder X-ray determination

Powder XRD data of the reported complexes were collected at room temperature over the whole collected crop of single crystals, previously carefully ground, with a Siemens D500 equipment using a graphite monochromated Cu ($\lambda = 1.54056$ Å) source. Five seconds integration time per each 0.02 degree step was used over the whole 8–30 (2 θ) range. Single crystal data were used to generate the simulated powder diffractogram which was in good agreement with the powder samples (see the ESI†).

Acknowledgements

We greatly acknowledge CONICET, ANPCYT and UBA for funding. PA is a staff member of CONICET. JvS and KB

thank the Fonds der Chemischen Industrie and DFG for funding.

References

- 1 T. N. Hooper, R. Inglis, M. A. Palacios, G. S. Nichol, M. B. Pitak, S. J. Coles, G. Lorusso, M. Evangelisti and E. K. Brechin, *Chem. Commun.*, 2014, **50**, 3498.
- 2 (a) X. J. Kong, Y. P. Ren, L. S. Long, Z. Zheng, R. B. Huang and L. S. Zheng, *J. Am. Chem. Soc.*, 2007, **129**, 7016; (b) X. J. Kong, Y. P. Ren, W. X. Chen, L. S. Long, Z. Zheng, R. B. Huang and L. S. Zheng, *Angew. Chem., Int. Ed.*, 2008, **47**, 2398.
- 3 D. Dermitzaki, G. Lorusso, C. P. Raptopoulou, V. Psycharis, A. Escuer, M. Evangelisti, S. P. Perlepes and T. C. Stamatatos, *Inorg. Chem.*, 2013, **52**, 10235.
- 4 (a) S. Du, Y. Bi, Y. Yi and W. Liao, *Sci. Sin.: Chim.*, 2012, **42**, 1356; (b) K. Xiong, X. Wang, F. Jiang, Y. Gai, W. Xu, K. Su, X. Li, D. Yuan and M. Hong, *Chem. Commun.*, 2012, **48**, 7456.
- 5 K. Liu, W. Shi and P. Cheng, *Coord. Chem. Rev.*, 2015, **289–290**, 74.
- 6 J.-L. Liu, Y.-C. Chen, F.-S. Guo and M.-L. Tong, *Coord. Chem. Rev.*, 2014, **281**, 26.
- 7 A. M. Ako, O. Waldmann, V. Mereacre, F. Klower, I. J. Hewitt, C. E. Anson, H. U. Gudel and A. K. Powell, *Inorg. Chem.*, 2007, **46**, 756.
- 8 (a) J. B. Peng, Q. C. Zhang, X. J. Kong, Y. Z. Zheng, Y. P. Ren, L. S. Long, R. B. Huang, L. S. Zheng and Z. Zheng, *J. Am. Chem. Soc.*, 2012, **134**, 3314; (b) S. Sakamoto, T. Fujinami, K. Nishi, N. Matsumoto, N. Mochida, T. Ishida, Y. Sunatsuki and N. Re, *Inorg. Chem.*, 2013, **52**, 7218; (c) S. Sakamoto, S. Yamauchi, H. Hagiwara, N. Matsumoto, Y. Sunatsuki and N. Re, *Inorg. Chem. Commun.*, 2012, **26**, 20.
- 9 (a) S. Akerboom, E. T. Hazenberg, I. Schrader, S. F. Verbeek, I. Mutikainen, W. T. Fu and E. Bouwman, *Eur. J. Inorg. Chem.*, 2014, **2014**, 4896; (b) V. Velasco, D. Aguilà, L. A. Barrios, I. Borilovic, O. Roubeau, J. Ribas-Ariño, M. Fumanal, S. J. Teat and G. Aromí, *Chem. Sci.*, 2015, **6**, 123.
- 10 S. Alvarez, P. Alemany, D. Casanova, J. Cirera, M. Llunell and D. Avnir, *Coord. Chem. Rev.*, 2005, **249**, 1693.
- 11 A. Abraham and B. Bleaney, *Electron Paramagnetic Resonance of Transition Ions*, Oxford University Press, 1970.
- 12 N. F. Chilton, R. P. Anderson, L. D. Turner, A. Soncini and K. S. Murray, *J. Comput. Chem.*, 2013, **34**, 1164.
- 13 M. Pait, A. Bauzá, A. Frontera, E. Colacio and D. Ray, *Inorg. Chem.*, 2015, **54**, 4709.
- 14 (a) M. Fondo, N. Ocampo, A. M. García-Deibe, R. Vicente, M. Corbella, M. R. Bermejo and J. Sanmartín, *Inorg. Chem.*, 2006, **45**, 255; (b) J. P. Wikstrom, A. S. Filatov, E. A. Mikhalyova, M. Shatruck, B. M. Foxman and E. V. Rybak-Akimova, *Dalton Trans.*, 2010, **39**, 2504.
- 15 L. Rosado Piquer and E. C. Sañudo, *Dalton Trans.*, 2015, **44**, 8771.
- 16 G. Chaboussant, R. Basler, H. U. Gudel, S. Ochsenein, A. Parkin, S. Parsons, G. Rajaraman, A. Sieber, A. A. Smith, G. A. Timco and R. E. P. Winpenny, *Dalton Trans.*, 2004, 2758–2766.
- 17 SCALE3 ABSPACK: Empirical absorption correction, *CrysAlis – Software package*, Oxford Diffraction Ltd., Oxford, 2006.
- 18 A. Altomare, M. C. Burla, M. Camalli, G. L. Casciarano, C. Giacovazzo, A. Guagliardi, A. G. G. Moliterni, G. Polidori and R. Spagna, *J. Appl. Crystallogr.*, 1999, **32**, 115.
- 19 G. M. Sheldrick, *Acta Crystallogr., Sect. C: Cryst. Struct. Commun.*, 2015, **71**, 3.
- 20 L. J. Farrugia, *J. Appl. Crystallogr.*, 2012, **45**, 849.
- 21 A. L. Spek, *Acta Crystallogr., Sect. C: Cryst. Struct. Commun.*, 2015, **71**, 9.